The impact of vortical flow on the free rolling motion of a delta wing aircraft

M.T. Arthur
QinetiQ Ltd.,
Cody Technology Park,
Ively Road,
Farnborough, Hampshire,
GU14 0LX
mtarthur@qinetiq.com

Abstract. This paper reports recent work undertaken within a collaborative programme concerned with the development of computational methods for the prediction of vortical flows. A strong feature of the programme has been the inclusion of both experimental and computational components and the close collaboration between the respective participants. The way in which the contributions of each side have enhanced the benefits to the other and thus to the programme as a whole is described. The important factors are highlighted through a discussion of an investigation of the vortical flow over a delta wing configuration in rolling motion. The investigation consisted of a series of validation exercises concerned with the unsteady, viscous or inviscid flow over the configuration undergoing a variety of forced and free motions. To illustrate the substantial progress that has been made, results for the free rolling motion of the configuration at incidence are presented.

Keywords. Unsteady, Navier-Stokes, flight mechanics, delta wing, free rolling motion

1. Introduction

The work presented here concerns parts of collaborative programmes on the development of computational methods for the prediction of vortical flows associated with military aircraft configurations. The programmes have been run under the auspices of the Western European Armaments Group (WEAG). The current programme is known as THALES Joint Programme 12.15 (JP12.15) and its predecessor was TA15. The partners are the UK (QinetiQ and the University of Glasgow), Germany (DLR and EADS(M)), The Netherlands (NLR) and Italy (Alenia).

In the TA15 programme, the vortical flow over a delta wing configuration undergoing forced oscillations in pitch was investigated[1]. In the last phase of the TA15 programme, and within JP12.15, the vortical flow over a delta wing configuration in rolling motion has been studied[2,3]. The studies formed important contributions to the validation of the computational methods as they were being developed. At the time the calculations were performed, therefore, they were at the limits of the computational experience of the participants. Comparisons of the computed results from the different participants were valuable in identifying inadequacies in algorithms or computational models, but validation against high quality experimental data was essential if the codes were to be brought into practical use. At the same time, obtaining the right data, of sufficient quality, was a considerable challenge. Computational results were used to inform the experimentalists and guide them to those parts of the configuration surface or flow field from which data would be of the greatest value. Significant differences between computed and experimental results were used to guide investigations of experimental technique and computational methods to the benefit of both sides on different occasions. In addition, the frequencies of forced motions, and the flow onset and initial conditions required to obtain particular types of behaviour were sometimes suggested by computational investigations. Furthermore, these initial computational investigations were shared out amongst participants in order to complete the studies more quickly and at limited cost to each partner. The result was that a greater volume of useful validation data could be obtained, maximising the value of the wind-tunnel tests. This close co-operation has proved to be an efficient and effective way of developing and validating capability.

The investigation of the rolling motion of the delta wing configuration provides a good example of the close co-operation between the experimental and computational contributors to the programme. Over a period of time a range of computations has been completed and several wind-tunnel tests have been performed. In an initial exercise, the inviscid, transonic flow over the configuration rolling about the fuselage axis was computed. Calculations for an angle of incidence of 0^o were used to verify that the time-varying terms had been incorporated into the flow prediction codes correctly (since for this case the flow is steady but asymmetric). Subsequent calculations were for angles of incidence of 10^o and 17^o at the maximum roll rate that could be realised in the wind tunnel at that time (10 revolutions per second), and at 10^o for a much higher roll rate to increase the unsteady effects of the rotation. Wind-tunnel measurements were made using pressure sensitive paint (PSP) in order to provide a large volume of surface data comparable with that obtained in the computations. It was recognised from the outset that the experiment posed a huge challenge. The fuselage had to be sufficiently large for the model to be mounted in the tunnel on a rig that enabled the model position to be controlled accurately and unwanted movement to be minimised. At the same time, interference between the wing flow being studied and vortical flow from the fuselage had to be eliminated or minimised. Thus the fuselage diameter falls smoothly to zero as the apex of the wing is approached and no part of the fuselage is ahead of the wing. The fuselage is blended smoothly to the wing surface to aid the illumination of the PSP. In addition, a small number of pressure transducers was used to check the response times of the paint and to aid the calibration. Great care was taken both in the illumination of the model surface and in the recording of images. Two cameras were used so that the upper surface could always be seen. However, combining the images was not straightforward since the model position had first to be known accurately and even then the mapping of the two-dimensional image to the three-dimensional surface was not straightforward. Furthermore, multiple images from a given roll angle were combined to produce the final result for that angle. Computed solutions aided the validation of the data reduction process and improvements to the process continue to be made.

In a second exercise, the steady, viscous flow was first computed for comparison with PSP data to provide confidence in the prediction methods. The unsteady, viscous flow for a case from the first exercise ($\alpha=17^o$, 10 rotations per second) was then computed in order that the importance of viscous effects could be assessed. Finally in that series of calculations, the flow over the configuration rolling about the wind axis was computed. This was more representative of the rolling motion of an aircraft in flight but very difficult to simulate in a wind tunnel.

In the final exercise undertaken to date, the free rolling motion of the configuration has been investigated. The governing flow equations have been augmented by a one-degree-of-freedom equation of motion of the vehicle in the computational methods of the partners, and new validation data has been obtained in carefully planned and performed experiments in the DNW transonic wing tunnel at DLR, Göttingen (TWG), as part of the DLR AeroSUM programme. THALES JP12.15 has highlighted the difficulties of simulating the motion of an air vehicle both numerically and in a wind tunnel. It is not possible to simulate free flight in a wind tunnel since there will always be mechanical friction in the moving parts of the model support rig. Moreover, it is extremely difficult to determine the friction law for the rig. Obtaining accurate measurements of the forces and moments on the moving model in the wind tunnel while tracking the model position and obtaining flow-field visualisation data hold many challenges. At the same time, it is to be expected that the details of the vehicle motion predicted by the different computational methods will differ since the motion is obtained from the integration of an equation containing aerodynamic moments. Small variations in these moments will produce a cumulative effect on the motion so that predictions from different methods may depart from each other increasingly with time. Nonetheless, if the motion is damped, the essential behaviour and the final, stable attitude may be predicted with greater reliability. If the motion is undamped, knowledge of that fact alone is very valuable, regardless of the precise details of the departure from controlled flight. However, it is possible to incorporate any friction law in the computational model, including none, thereby enabling free flight to be simulated and providing a bridge linking the two quite different experimental techniques, allowing differences between flight test and tunnel results to be reconciled.

In order to demonstrate the capability that has been developed and the benefits of close co-operation between experimental and computational participants, a selection of results from the investigation of free rolling motion will be presented. The configuration adopted for the investigation and the grid used for the computations are first described. An outline description of the different computational methods used by the participants is provided. The equation of motion of the vehicle is then described. Vehicle motions for three sets of boundary and initial conditions are considered. The conditions are defined and the reasons for choosing them are explained. Some preliminary calculations that were performed to determine a suitable value for the computational time step length and the form of the model of the mechanical friction law for the tunnel support rig are described briefly. The main results are then presented. The flow development is described and related to the observed vehicle motion. Finally, some conclusions are drawn and a comment is made about the wider significance of the work.

2. Description of configuration and computational grid

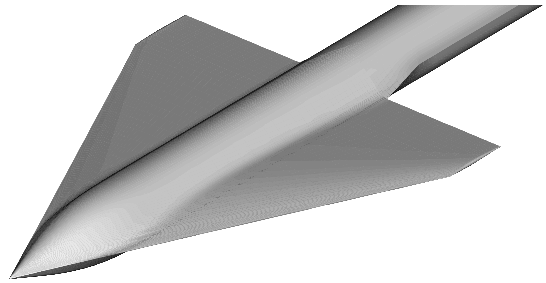

Figure 1 Model geometry

The configuration adopted for the investigation was used in the previous studies of the flow over rolling delta wings within THALES JP12.15[3] and WEAG TA15[2]. The wing has a sharp leading edge with 65° sweep and a cropped tip. It is mounted symmetrically on a fuselage of which the cross-section is circular except that it is blended smoothly into the surface of the wing. For the computations, the fuselage is blended and tapered to the smaller circular cross-section of the sting, the trailing edge thickness is reduced smoothly to zero and the wing tip has been rounded. The model geometry is shown in figure 1.

A single block grid of C-O topology, generated by EADS(M), was used by all participants except Alenia, who used a coarsened version of the grid obtained by omitting alternate points in the chordwise and spanwise directions. On the wing surface, the grid is conical, all members of one set of grid lines (the 'C' lines) passing through the apex of the wing while each member of the other set is at a constant value of the streamwise co-ordinate, x. There is a singular line from the apex to the upstream far-field boundary and O-type singularities on each side from the wing tip trailing edge to the downstream far-field boundary. There are 144 intervals in the streamwise direction from the apex, 320 in the circumferential direction around the wing and 64 in the normal direction from the wing surface to the far-field boundary, yielding a total of 2,949,120 cells. The grid was designed to provide sufficient resolution of the viscous layers and to suit the vortical flows associated with delta wings while at the same time taking account of the practical limitations of available computer resources.

3. Numerical methods

The governing flow equations are taken to be the Reynolds-averaged Navier-Stokes equations together with an appropriate turbulence model. Several turbulence models have been employed within the TA15 and JP12.15 programmes although only three have been used to obtain the results presented here. Three participants used a variant of the Wilcox k-ω model[4], developed at NLR[5]. It is known that the standard model is too diffusive in the region of vortex cores. In the modified form, the ratio of the magnitude of the strain rate tensor to the magnitude of the vorticity is used as a sensor for vortex cores and hence to control the production of eddy viscosity through an increase in the production term in the ω equation. This has the effect of increasing the dissipation of turbulence kinetic energy and hence reducing the eddy viscosity. Alenia used both a k-R_t model and an explicit algebraic Reynolds stress model (EARSM). Jameson's dual time-stepping formulation was used in all the methods to obtain time accuracy.

PMB3D, the code developed by and used at the University of Glasgow, is a cell-centred, finite-volume method using Osher's upwind distribution of residuals for the convection terms. MUSCL extrapolation is used to provide second-order accuracy. An implicit time marching scheme is used to obtain the solution at each real time step. The turbulence model equations are solved in a similar manner to that employed for the mean flow equations.

The FLOWer code was used at EADS(M). It is a cell-vertex, finite-volume method of Jameson type. An anisotropic form of artificial dissipation is employed; the dissipation terms are scaled by functions of the convective eigenvalues in each direction for each control volume. The mean flow and turbulent transport equations are solved simultaneously during each time step.

The ENFLOW code used at NLR solves the turbulence model and mean flow equations as a single system. It is a cell-centred, finite-volume method employing a matrix artificial dissipation scheme which appears to yield improved accuracy inside the boundary layers. Both the FLOWer and ENFLOW codes use a Runge-Kutta time-stepping scheme, and local time-stepping, implicit residual averaging and multigrid to improve the rate of convergence at each real time step.

The UNS3D code used at Alenia is a vertex-centred, finite-volume method designed for irregular grids. An artificial dissipation scheme has been derived from the non-linear scheme of Jameson to suit the irregular structure of the computational cells. Runge-Kutta time-stepping is again used to obtain the solution at each real time step. Local time-stepping and implicit residual averaging are used to speed convergence but multigrid acceleration is not used. The method solves the mean flow and turbulence transport equations in a similar manner.

4. Equation of motion of the vehicle

In this initial study of the feasibility of predicting the free manoeuvre of an air vehicle under aerodynamic load, the Navier-Stokes equations governing the unsteady flow have been augmented by a simple model of the vehicle motion in which the vehicle is free to roll about the fuselage axis. The equation governing the motion is therefore

$$I_\phi \, \phi_{tt} = L(\phi, \phi_t)$$

where I_ϕ is the moment of inertia of the model about the fuselage axis, ϕ is the roll angle, L is the couple producing the motion and t is time. Here, L includes the aerodynamic moment and the effect of mechanical friction in the model support.

It is convenient to write the equation in a dimensionless form consistent with the flow solution code. Let

$$I_\phi = mr_\phi^2 = mR_\phi^2 c_{ref}^2 ,$$

and

$$L(\phi, \phi_t) = \frac{\rho_\infty u_\infty^2}{2} S \left(C_l(\phi) - \overline{C}_{lf}(\phi, \phi_t) \right) l_r .$$

The mass of the model is m, R_ϕ is the radius of inertia scaled by the reference chord, c_{ref} , S is a wing reference area and l_r is the moment arm used to define the rolling moment. The free stream speed and density of the air are u_∞ and ρ_∞ respectively. C_l is the aerodynamic rolling moment coefficient while $\overline{C}_{lf}$ is the roll moment damping coefficient due to mechanical friction. It is written in a general form as a function of the roll angle and roll rate. The equation of motion may then be written in non-dimensional form as

$$\phi_{\tau\tau} = \frac{\gamma M_\infty^2}{\mu R_\phi^2} \left(C_l(\phi) - \overline{\overline{C}}_{lf}(\phi, \phi_\tau) \right),$$

in which it has been assumed that $p_\infty = \rho_\infty = 1$ so that $u_\infty = \gamma M_\infty$ in the units of the flow solution code, and μ is a non-dimensional mass, $\mu = 2m/\rho_\infty S l_r$. It is in this form that the model is best suited to coupling to the Navier-Stokes flow solvers.

In free flight, $\overline{\overline{C}}_{lf}$ is, of course, zero. In the wind tunnel, however, it is non-zero but its form and magnitude are difficult or impossible to determine with confidence. Thus several mathematical models of the mechanical friction law and values of coefficients were explored computationally in an attempt to reproduce the vehicle motions observed in the wind tunnel for a range of cases. The form found to give the best results overall was the simplest possible, constant mechanical friction. Since it always acts so as to oppose the motion, it is taken to be $\overline{\overline{C}}_{lf}(\phi, \phi_\tau) = C_{lf} \, sign(\phi_\tau)$. A coefficient $C_{lf} =$ 3Nm was found to give good overall agreement with experiment. This form of mechanical friction is, of course, discontinuous at $\phi_\tau = 0$. Some care is therefore needed in implementing the model and one approach that has been explored is to smooth the discontinuity, replacing $C_{lf} \, sign(\phi_\tau)$ by $2 C_{lf} \arctan(k_0 \phi_\tau)/\pi$. The form in which the mechanical friction model is implemented can have a significant effect on the solution.

It should be noted that during the predicted motion of the vehicle, there is a possibility that ϕ_τ will become zero while $|C_l(\phi)|$ is less than C_{lf} . The computational model has been implemented in all the codes so that, should this circumstance arise, ϕ_τ will remain zero, i.e. the motion will cease.

5. Description of the test cases and preliminary studies

Three examples of rolling motion have been investigated, one in which no vortex breakdown is observed experimentally and two in which vortex breakdown does occur and has a significant impact on the vehicle motion. In all cases, the vehicle, at incidence, is released from rest at a non-zero roll angle, ϕ_0, and is free to move in roll. The flow over the vehicle, which produces the ensuing motion, is determined by the instantaneous angles of incidence and yaw, and by the movement of the vehicle, in addition to the free stream conditions. The angles of incidence and yaw change continuously during the motion. Various distinct types of damped vehicle motion might be expected to lead to one of three different final states depending on the initial conditions, although the conditions which lead to a given state will be different in free flight and a wind tunnel because of the mechanical friction in the tunnel support rig. In the cases studied here, the initial flow over the wing produces a restoring rolling moment so that the roll angle, ϕ, will decrease after the vehicle is released. The simplest type of motion is that in which the model oscillates about the symmetric position, $\phi=0^o$, and eventually comes to rest there in steady flow. A second final state is one in which the vehicle comes to rest at a non-zero roll angle, ϕ_1, with ϕ_1 the same sign as ϕ_0. This can arise if vortex breakdown occurs, leading to a loss of lift from the rear of a wing which compensates high lift from the strong vortex above the forward part of the wing and balances the lift induced by the weaker vortex above the wing on the opposite side resulting from the change in incidence and yaw at a non-zero roll angle. A third final state is one in which the vehicle comes to rest on the opposite side to that on which it began the motion, at roll angle $\phi_2=-\phi_1$. There are several different types of motion which can lead to these states, some of which will be seen in the results which follow. There may, in addition, be undamped motions and instabilities. The flow onset and initial conditions for the three examples for which results are presented have been chosen because they produce motions leading to each of the stable final states described above.

Some preliminary studies were undertaken before the examples were computed by all participants in the programme. Earlier work on the prediction of the flow over a vehicle undergoing forced rolling motion suggested that a suitable time step length which would ensure independence from the time step length in the computed solutions was such that the predicted change in roll angle was no more than 5^o per (real) time step. However, studies of the free rolling motion suggested that a shorter time step would be required, with the roll angle changing by no more than 2.5^o per time step. In practice, it was found that for some methods, an even shorter time step led to faster convergence of the marching scheme in pseudo-time and a shorter computational time for the complete motion.

In addition, it was recognised that grid fineness studies should be undertaken, though it was also recognised that there were practical limitations on the mesh size that could be used. Calculations were performed on both the standard mesh and a coarsened version in which alternate points in each co-ordinate direction were omitted. Significant differences between the results were observed. A further calculation is currently being undertaken using a grid which has twice the number of intervals in both the spanwise and chordwise directions, and a final calculation using a grid which has twice the number of intervals in each co-ordinate direction (approximately 24 million cells in total) is planned.

6. Results

All the examples studied were for transonic flow, $M_\infty=0.85$. For the first case, the (maximum) angle of incidence was 9^o, the Reynolds number was 4.9×10^6 and the initial roll angle was 40^o (i.e. with the port wing down). The objective was to simulate the behaviour in 'free flight' (with just one degree of freedom) and so the coefficient of mechanical friction was set to zero. However, experimental data were available for the same initial roll angle and flow conditions and so an additional calculation in which mechanical friction was included was undertaken at EADS(M) so that the vehicle motion could be compared with that observed in the experiment. Figure 2 shows the distribution of computed surface pressure at four spanwise stations at the start of the motion. In addition, at stations 2 and 3, experimental results are shown. The figures are viewed as if from ahead of the aircraft so that the port wing is on the right, $\eta>0$. The computed flow separates at, or close to, the leading edge and vortices develop above both halves of the wing. The vortex above the port wing computed by EADS(M) and Glasgow is well developed and produces a large suction on the surface close to the leading edge. However, a much weaker vortex is predicted by both Alenia and NLR. Only in the solution from EADS(M) is the vortex strength maintained over the rear part of the wing. There are additional, minor suction peaks on the forward part of the wing. The inboard peak seen in the experimental data and all the predictions, but most noticeably in that from Alenia, is most likely an effect of the high relative thickness of the fuselage in this region. The outboard peak, very close to the leading edge, is most apparent in the solutions of EADS(M) and Alenia and is the result of a secondary separation induced by the primary vortex. There is a hint of this in the experimental pressure distribution at 60% chord and $\eta \approx 0.82$. However, the experimental pressure distribution at this station shows a very different character from the computed solutions and suggests a different flow development. There is an additional suction peak outboard. The explanation is not yet clear but it may be that the flow is attached outboard of 85% semispan; it may separate at that point and then reattach at 60% semispan. The high outboard suction peak would then be the conventional leading edge suction peak associated with attached flow. If this description is correct, the experimental data at 80% chord suggest that the primary separation line has moved close to the leading edge with reattachment at 72% semispan. The fact that none of the computed solutions reproduces this behaviour is a cause for concern. It is unlikely to be the result of a deficiency in the turbulence model since such behaviour has not been observed in solutions obtained with any of the turbulence models used by participants, a much wider range than used to produce the results presented here. Furthermore, the turbulence models are not noted for the early prediction of separation in other flows. More likely is it that the leading edge of the wind-tunnel

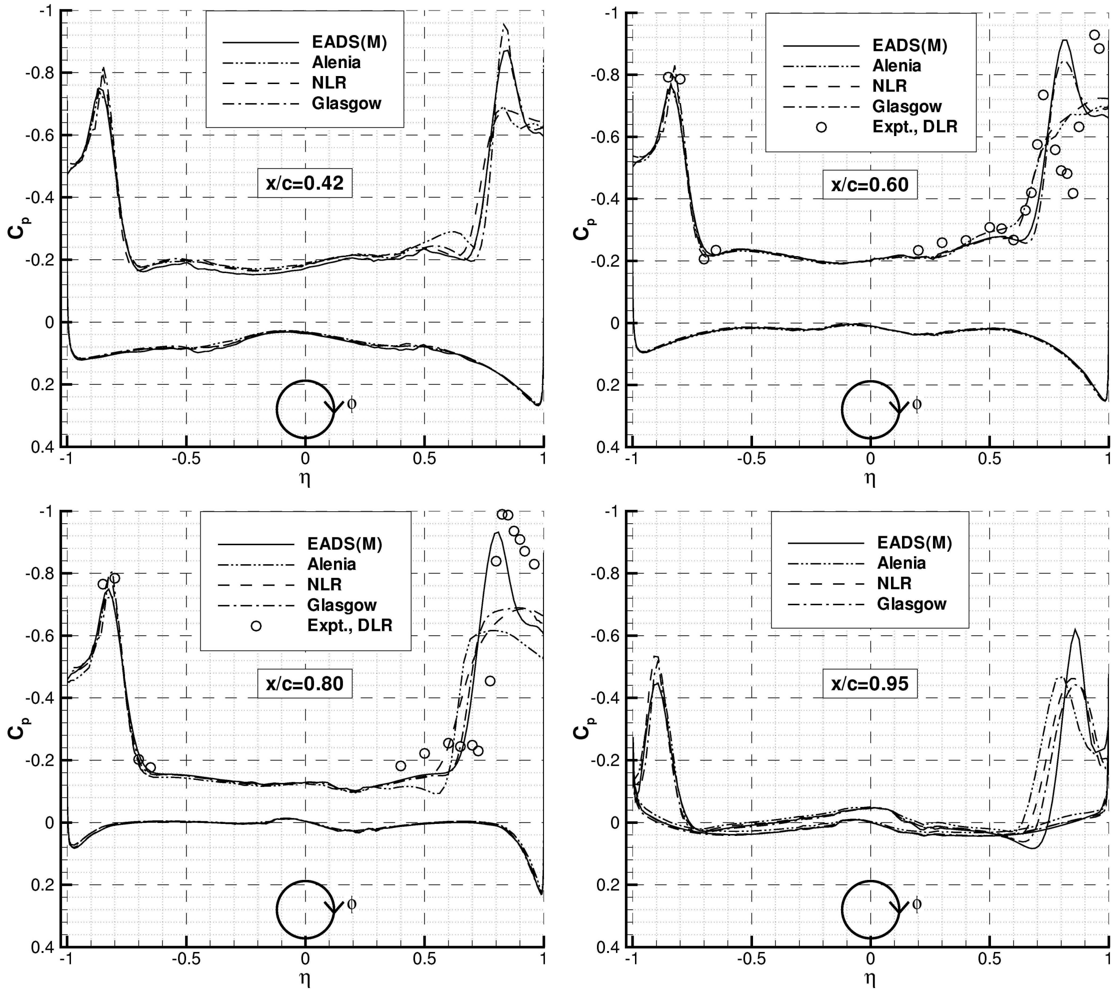

Figure 2 Case 1: Spanwise distribution of surface pressure coefficient M_∞=0.85, α=9^o, Re=4.9x10^6, ϕ_0=40^o

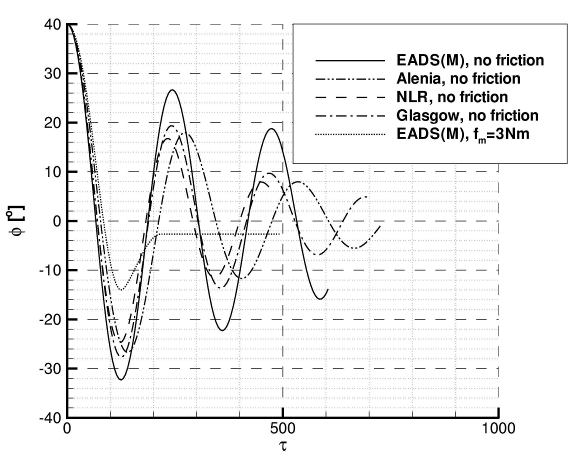

Figure 3 Case 1: Variation of roll angle with computational time

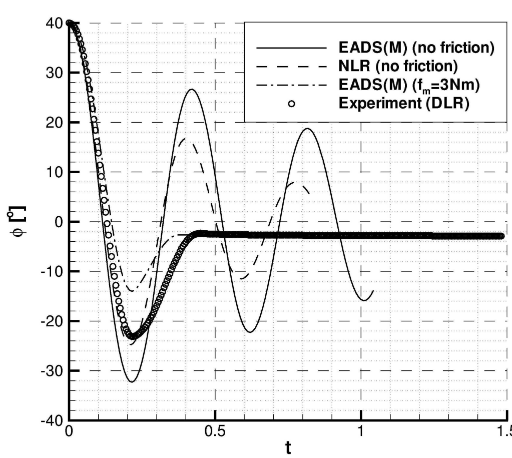

Figure 4 Case 1: Variation of roll angle with true time

model is not truly sharp as it is in the computational model. It is also possible that the early separation in the computed flows arises from an inadequacy in the fineness of the grid in the leading edge region. Some evidence of this was seen in an earlier exercise in the TA15 programme[6]. Certainly, the computed viscous flow can remain attached around the sharp leading edge.

Figure 3 shows the variation of roll angle with computational time predicted by the various methods. The vehicle undergoes damped oscillations about $\phi=0$, at which it will eventually come to rest. There is fair agreement between the results. The compact, well-developed vortices of the EADS(M) solution are associated with lower aerodynamic damping and hence a larger amplitude of oscillation, while the grid refinement calculations described earlier suggest that the lower frequency of the solution predicted by Alenia is caused by the use of too coarse a grid. The figure also shows the result from EADS(M) which includes mechanical friction.

Figure 4 shows the same solutions from NLR and EADS(M) plotted against real time, and also the motion observed in the wind tunnel. The general form of the motion predicted by EADS(M) with mechanical friction included agrees with the behaviour observed in the tunnel. A smaller coefficient of friction may have produced better agreement in amplitude, but this computational model and coefficient gave the best agreement with experiment across the range of cases studied. Note that, in both the EADS(M) prediction and in the experiment, the angular velocity of the model falls to zero, with c_l<3Nm, when $\phi \neq 0$. The model therefore remains in that position.

The angle of incidence was increased to 17^o for the second case and the configuration was released from rest at roll angle 30^o. Mechanical friction as described in section 4 was included in all computations. Figure 5 shows the computed surface pressure distributions at the same stations as for case 1. No experimental pressure data are available for this case. All the methods show a well-developed primary vortex above the starboard wing with a clear secondary separation. They also show a strong vortex above the forward part of the port wing, with an associated secondary vortex. In all cases, the primary vortex breaks down between 60% and 80% chord. There is good agreement in the predicted location of vortices and in the values of peak suctions though there is some variation in the predicted location of vortex breakdown. A region of higher pressure inboard is associated with the vortex burst and this can be seen in the pressure distributions. The solutions form two groups, with breakdown occurring slightly further forward in the results from Glasgow and EADS(M) than in those from NLR and Alenia. However, the peak suctions are much higher than those for case 1 over the forward part of the wing, as one would expect at this higher angle of incidence, and so the initial rolling moment is also significantly higher. The resultant motion of the model is shown in figures 6 and 7. Two distinct types of behaviour have been predicted. All participants predict that the vehicle begins to accelerate towards the symmetric position, $\phi=0$, but then decelerates and comes to rest before reaching that position. It then accelerates back towards its initial position. Alenia and EADS(M) predict that ϕ increases to approximately 11^o as the angular velocity falls to, and remains at, zero. Examination of the surface pressure distribution indicates that there is vortex breakdown above the port wing leading to a loss in lift over the rear of the wing which, together with the high lift over the forward part of the wing, produces a rolling moment that exactly balances that from the starboard wing, providing a stable or trim position. In contrast, Glasgow and NLR predict that the roll angle increases to only about 7 or 8^o. The vehicle comes to rest but the flow continues to develop; the magnitude of the rolling moment begins to increase again and the vehicle moves towards the symmetric position, $\phi=0$, at which it finally comes to rest. Figure 8 shows the variation of angular velocity with computational time. It can be seen that the peak magnitudes of ϕ_τ predicted by Glasgow and NLR in both halves of the cycle are smaller than those predicted by EADS(M). The angular momentum generated during the second half of the cycle is therefore insufficient to carry the vehicle towards the trim point $\phi \approx 11^o$ and it is 'captured' by the trim point in symmetric flow. The vortex above the port wing has re-established itself in these predictions. The results are consistent with those obtained for case 1 in which the narrower vortex cores of the EADS(M) solution led to lower aerodynamic damping and thus larger amplitudes of oscillation. The experimental result, shown in figure 7, is in good agreement with the prediction from EADS(M). The prediction from Alenia is probably fortuitous in that the peak magnitude of the angular velocity was the lowest of all the predictions and so the vehicle was 'captured' by the trim position $\phi \approx 11^o$ at the first pass with only slight overshoot. It is likely that this is a consequence of the coarse grid used for the calculation though further investigation is necessary.

Analysis of the available experimental data reveals that the initial conditions are very close to conditions for which the vehicle motion changes character, essentially from that predicted by EADS(M) and observed in the experiment to that predicted by Glasgow and NLR. The differences between these two sets of results should therefore not be regarded as failures of the methods of Glasgow or NLR, but rather as an indication of the sensitivity of the vehicle motion to the initial conditions. An improvement to the turbulence model or its implementation, or a modified form for the mechanical friction, may well lead to the recovery of the observed behaviour, but it is most unlikely that any of the methods of the partners would reproduce the observed vehicle motion for the complete range of initial roll angles for which experimental results were obtained.

The conditions for the third case were similar to those for case 2 except that the initial roll angle was 60^o and the Reynolds number was reduced slightly, to 4.8x10^6, in accordance with the experimental conditions. The effective

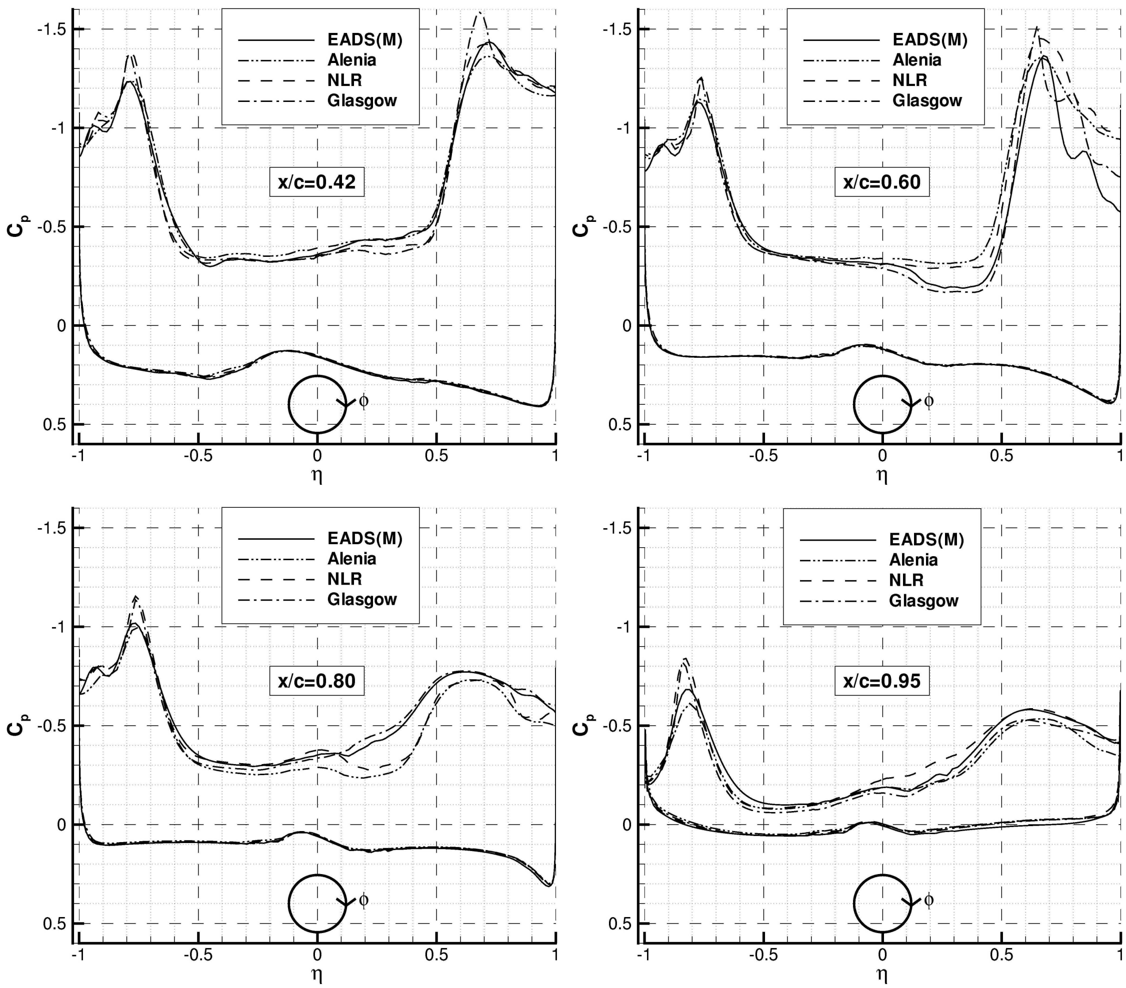

Figure 5 Case 2: Spanwise distribution of surface pressure coefficient M_∞=0.85, α=17^o, Re=4.9x10^6, ϕ_0=30^o

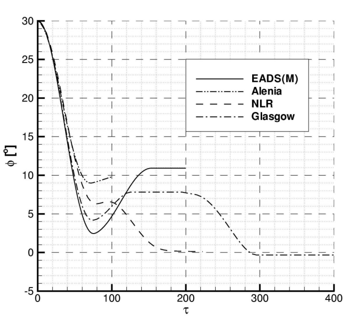

Figure 6 Case 2: Variation of roll angle with computational time

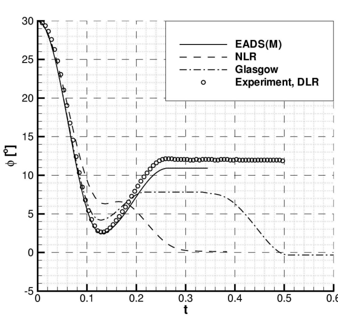

Figure 7 Case 2: Variation of roll angle with true time

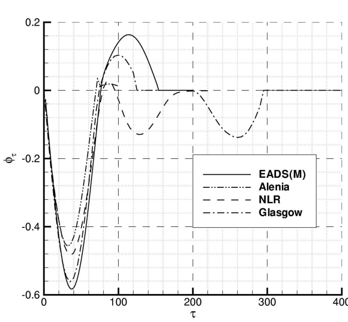

Figure 8 Case 2: Variation of angular velocity with computational time

angle of incidence at the start of the motion is quite small and so the vortex above the starboard wing is very weak, as shown in the spanwise distributions of surface pressure coefficient, figure 9. Glasgow and EADS(M) predict a vortex over the port wing , although it is broad and weak by 80% chord. The figure suggests that the flow predicted by Alenia and NLR may be attached at the leading edge over much of the wing, though further investigation will be required to confirm this topology. The strong asymmetry in the flow leads to a higher initial rolling moment than for case 2 despite the lower peak suctions. The predicted motion is shown in figures 10 and 11. As in case 2, the vehicle accelerates towards the symmetric position, ϕ=0, but the higher initial rolling moment generates sufficient angular momentum to carry the vehicle through the trim positions at both $\phi \approx 11^o$ and $\phi \approx 0^o$. It comes to rest momentarily at a minimum roll angle of almost -30^o, close in magnitude to the initial value for case 2. The vehicle then moves back towards the symmetric position. EADS(M) and NLR predict that the vehicle comes permanently to rest at a third trim position, $\phi \approx -11^o$. This is symmetric with the trim position found in case 2 and results from a balance of moments associated with vortex breakdown over the starboard wing. The second part of the motion of the vehicle, after the minimum value of ϕ has been attained, closely resembles that predicted by EADS(M) for case 2. The motion predicted by Glasgow is again a little different, the higher peak angular velocity allowing the vehicle to pass through the trim position at $\phi \approx -11^o$ and to be 'captured' by the symmetric trim state. Note that the final roll angle predicted by Glasgow differs slightly from $\phi \approx 0^o$ and the final angles predicted by EADS(M) and NLR differ slightly from each other because of the constant mechanical friction included in the equation of motion. The motion predicted by EADS(M) and NLR agrees well with that observed in the tunnel, shown in figure 11.

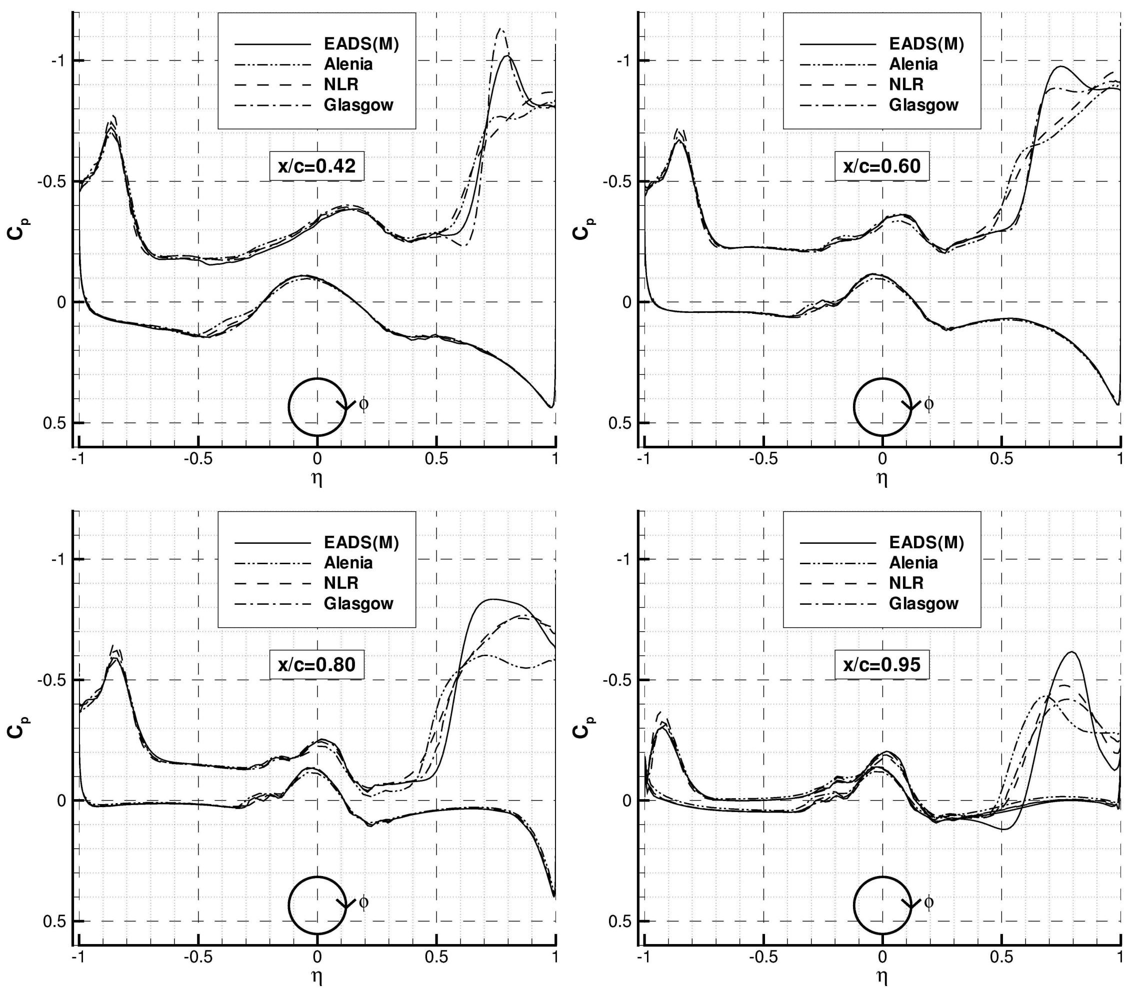

Figure 9 Case 3: Spanwise distribution of surface pressure coefficient
M_∞=0.85, α=17^o, Re=4.8x10^6, ϕ_0=60^o

The final flow and surface pressures predicted by EADS(M) and NLR are mirror images of those for case 2, as one would expect. The result from Glasgow is more interesting. It might be expected that the final flow predicted by Glasgow is the same for all three of the cases studied but that turns out not to be so. Figure 12 shows the predicted distribution of surface pressure at the end of the motion. It is clear that vortex breakdown has occurred above both wings. During the early part of the motion, the vortex above the starboard wing grows in strength and eventually breaks down after the minimum value of ϕ is reached. It never recovers. However, as the vehicle approaches its final position, at $\tau \approx 200$, the vortex above the port wing breaks down and a near-symmetric flow is established, different from that of case 1. The associated lift, drag and pitching moments are therefore also very different in the two cases. The result indicates once again the sensitivity of the vehicle motion to the initial and flow onset conditions, and hence to small variations in the predicted flow from different methods. It suggests that there is a set of initial and flow onset conditions, not very different from those of this case, for which the motion of the model in the tunnel would be similar to that predicted by Glasgow.

Figures 10 and 11 include an additional result. It shows the vehicle motion predicted by EADS(M) for free flight (i.e. without the mechanical friction of the wind tunnel support rig) for the same initial and flow onset conditions. It can be seen that the vehicle will eventually come to rest at $\phi \approx 11^{o}$, the trim position found for case 2 with mechanical friction included. This indicates that the trim positions found for cases 2 and 3 are not peculiar to wind tunnel experiments; they apply equally to the vehicle in free flight. The motions observed in the wind tunnel and in free flight will be different for a given set of conditions, but the same types of behaviour will occur at different conditions and CFD can be used to help explain the observations.

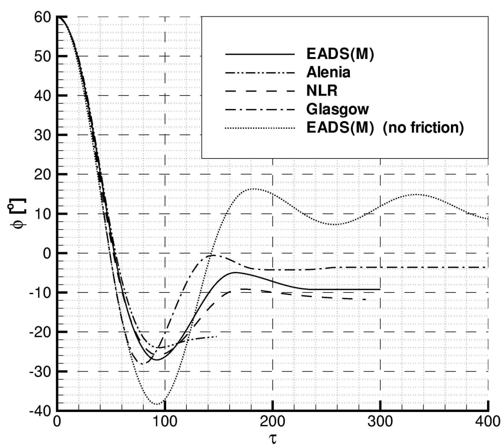

Figure 10 Case 3: Variation of roll angle with computational time

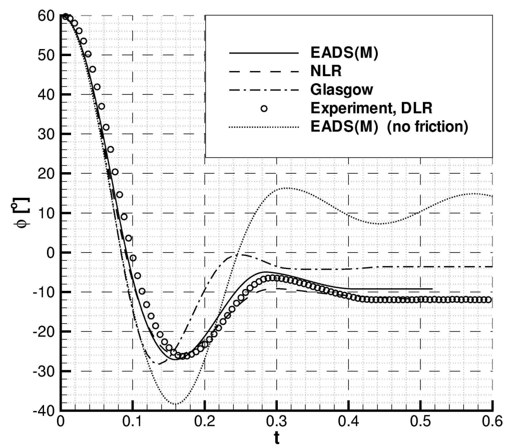

Figure 11 Case 3: Variation of roll angle with computational time

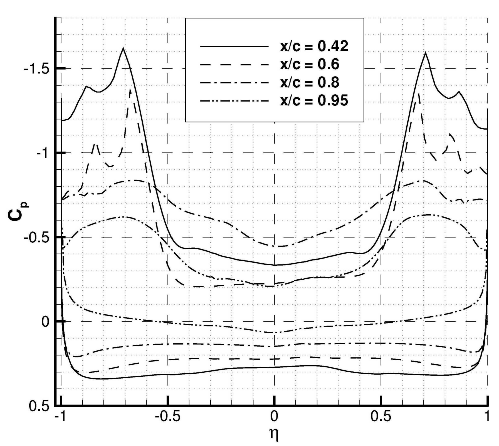

Figure 12 Case 3: Spanwise distribution of surface pressure coefficient at the end of the motion (University of Glasgow)

7. Conclusions

The objectives of the validation exercise have been met. Several methods for solving the Navier-Stokes equations governing unsteady flow have been augmented by a simple, one degree of freedom model of the motion of an air vehicle. Solutions of the complete set of equations have been obtained for a range of cases, and both spatial and temporal grid refinement studies have been undertaken. The methodology has been shown to be robust. Some of the damping characteristics of a delta wing configuration manoeuvring in roll have been explored.

The work represents a successful first step in the exploitation of CFD for the simulation of aircraft manoeuvre. The results demonstrate that important, non-linear behaviour of manoeuvring air vehicles can be simulated and, in particular, differences between free flight and wind tunnel results can be explored and explained. A calculation for a complete manoeuvre typically takes less than one day (wall clock time) on a p.c. cluster with 20 processors. The development of the capability to include a full six-degrees-of-freedom vehicle equation of motion is therefore feasible and very valuable: the computation time for simulating a complete manoeuvre is likely to be just a few hours by the time the capability is available and fully validated. The methods could then be used regularly in an analysis or assessment context. It will be possible to explore manoeuvres that are difficult to perform in a wind tunnel or dangerous to perform in flight. Further enhancements could allow the effects of control surface deployment to be investigated. This will aid the assessment of real vehicles and their control laws and hence also the design of flight simulators.

8. Acknowledgements

The author would like to thank the participants in the THALES JP12.15 programme who have contributed to the study described here, including W. Fritz (EADS(M)), J. Kompenhans (DLR), N. Ceresola (Alenia), O.J. Boelens and B. B. Prananta (NLR), and M. Allan and K.J. Badcock (The University of Glasgow), for allowing their results to be presented. The author would also like to thank Prof. D. Hummel for many very valuable discussions. The collaboration has greatly enhanced the value of the study to all participating organisations and, at the same time, has enhanced the value of the published results.

9. References

1. Arthur, M.T., Brandsma, F., Ceresola, N. and Kordulla, W, *Time accurate Euler calculations of vortical flow on a delta wing in pitching motion*, paper presented at the AIAA 17th Applied Aerodynamics Conference, 28th June – 1st July, 1999, Norfolk, Virginia, U.S.A., AIAA-99-3110.

2. Fritz, W., Arthur, M.T., Brandsma, F.J., Bütefisch, K.-A. and Ceresola, N., *Time accurate Euler calculations of vortical flow over a delta wing in rolling motion*. RTO/AVT Vortex Flow Symposium, Loen, Norway, 2001.

3. Soemarwoto, B.I., Boelens, O.J., Fritz, W., Allan, M., Arthur, M.T., Ceresola, N., and Bütefisch, K., *Towards the simulation of unsteady maneuver dominated by vortical flow*, AIAA 2003-3528, AIAA 21st Applied Aerodynamics Conference, June 2003.

4. Wilcox, D.C., *Turbulence modelling for CFD*, DCW Industries, 1998.

5. Brandsma, F.J., Kok, J.C., Dol, H.S. and Elsenaar, A., *Leading edge vortex flow computations and comparison with DNW-HST wind tunnel data*, RTO/AVT Vortex Flow Symposium, Loen, Norway, 2001.

6. Arthur, M.T., *WEAG TA15 Common Exercise III on grid adaptation in vortical flow simulations*, unpublished results, 1997.